J Appl Electrochem (2011) 41:1329–1340
DOI 10.1007/s10800-011-0351-7

ORIGINAL PAPER

Characterization of the performance and failure mechanisms of boron-doped ultrananocrystalline diamond electrodes

Brian P. Chaplin · Ian Wyle · Hongjun Zeng · John A. Carlisle · James Farrell

Received: 16 June 2011 / Accepted: 29 August 2011 / Published online: 25 September 2011

Abstract This research investigated the anodic stability of boron-doped ultrananocrystalline diamond (BD-UNCD) film electrodes on a variety of substrates (Si, Ta, Nb, W, and Ti) at a current density of 1 A cm^{-2}. At an applied charge of 100 A h cm^{-2}, measurable BD-UNCD film wear was not observed using SEM cross-sectional measurements. However, anodic treatment of the electrodes resulted in surface oxidation and film delamination, which caused substantial changes to the electrochemical properties of the electrodes. The substrate roughness, substrate electroactivity, and compactness of the substrate oxide were key parameters that affected film adhesion, and the primary mechanism of electrode failure was delamination of the BD-UNCD film. Substrate materials whose oxides had a larger coefficient of thermal expansion relative to the reduced metal substrates resulted in film delamination. The approximate substrate stability followed the order of: Ta > Si > Nb > W ≫ Ti.

Keywords Diamond film · Ultrananocrystalline · Electrode wear · Trichloroethylene

B. P. Chaplin (✉)
Department of Civil and Environmental Engineering, Villanova University, 800 E. Lancaster Ave., Villanova, PA 19085, USA
e-mail: brian.chaplin@villanova.edu

I. Wyle · H. Zeng · J. A. Carlisle
Advanced Diamond Technologies Inc., 429 B Weber Road, #286, Romeoville, IL 60446, USA

J. Farrell
Department of Chemical and Environmental Engineering, University of Arizona, 1133 E. James E. Rogers Way, Tucson, AZ 85721, USA

1 Introduction

Boron-doped diamond (BDD) film electrodes have recently gained attention for their usefulness for a variety of emerging electrochemical technologies. These applications include: (1) water disinfection and treatment, (2) electrochemical sensors, and (3) electro-synthesis of organic and inorganic compounds [1]. Traditional BDD synthesis results in films that are composed of boron-doped microcrystalline diamond (BD-MCD), with crystal sizes in the range of 0.5–10 μm [2, 3]. Although the electrochemical properties of BD-MCD are acceptable, the relatively large grain size can result in films that contain pinholes and defects that promote premature film delamination. The large grain size also prevents coverage of nanostructured materials by BD-MCD films, which prevents the coating of nanowires, carbon nanotubes, and nanoparticles and their subsequent use in emerging applications in electronics, medicine, and chemical and biochemical nanotechnology.

The development of ultrananocrystalline diamond (UNCD) films overcomes the primary problems associated with MCD films. UNCD films are highly uniform resulting from the small grain size of the material (2–5 nm) [4]. Work has shown that UNCD films are pinhole free and have lower residual stress than traditional MCD materials [4–7]. These unique properties have facilitated coverage of micro- and nano-electrochemical systems (MEMS/NEMS) [5, 7–9], and hold promise for other unique applications.

An additional problem associated with BDD electrodes is that the most compatible substrate is p-doped Si, because of the ability of Si to form a compact self-limiting oxide and its relatively low electrochemical activity. However, Si substrates are extremely brittle, and this limits its adoption in many applications.

The objective of this work is to test the performance and anodic stability of boron-doped ultrananocrystalline diamond (BD-UNCD) film electrodes as a function of the cumulative charge passed by each electrode. Specifically, the electrochemical, physical, and chemical properties of BD-UNCD films will be assessed on a variety of substrates (Si, Ta, Nb, W, and Ti) as a function of anodic ageing using scanning electron microscopy (SEM), Raman spectroscopy, X-ray photoelectron spectroscopy (XPS), cyclic voltammetry (CV), electrochemical impedance spectroscopy (EIS), and bulk oxidation of trichloroethylene (TCE). The results of this study will be used to characterize the mechanisms associated with electrode failure and develop stable anodes that can be used for a variety of electrochemical applications.

2 Materials and methods

2.1 Electrode preparation

Substrate materials consisted of 2-mm thick Si, Ta, Nb, W, and Ti metals, and were cut into 1.0-cm^2 circular disks using a water jet. The substrate surfaces were pretreated to promote the adhesion of diamond during the deposition process. Pretreatment consisted of roughening the surface with a proprietary method followed by seeding with nanodiamond to obtain a high density of nucleation sites. The chemical vapor deposition (CVD) process was performed using trimethyl borane (TMB) at concentrations of 750–12,000 ppm in flowing CH_4 at a temperature between 700 and 800 °C. The BD-UNCD film was grown to a thickness of approximately 2 μm. Typical resistivity measurements, by a Four Point Resistivity System (Lucas Labs Pro-4), were 0.05–0.1 Ω cm.

2.2 Reagents

All chemicals were reagent grade and were obtained from Sigma-Aldrich. Chemicals were used as received without additional purification. Background aqueous electrolyte solutions of K_2SO_4 and $NaClO_4$ were used for TCE oxidation experiments and electrode wear experiments, respectively. The Na_2SO_4 electrolyte was used to avoid Cl^- contamination present in $NaClO_4$ solutions, as Cl^- is a product of TCE oxidation. The $NaClO_4$ electrolyte was used because it has been shown to be nonreactive at BDD anodes and cathodes [10, 11]. All solutions were prepared from Milli-Q Ultrapure water (18.2 MΩ cm at 21 °C).

2.3 Electrode ageing experiments

Electrode ageing experiments were conducted in 200 mL Pyrex® beakers. Circular 1-cm^2 BD-UNCD electrodes were mounted into custom PEEK® electrode holders. Electrical contact was made with the backside of the electrode using a 316 stainless steel current collector contained within the electrode holder, and a water-tight seal was accomplished by sealing the face of the electrode with a Viton® gasket. The cell holder provided a 0.35-cm^2 area exposed to the solution. The BD-UNCD electrode was used as the anode and was held stationary in the middle of the reactor. A 316 stainless steel mesh screen was wrapped around the inner diameter of the reactor and was used as the cathode. The background electrolyte was 1-M $NaClO_4$ and was continuously stirred using a magnetic Teflon-coated stir bar. The electrodes were connected to a MASTECH (Hong Kong) model HY1803D galvanostatic power supply operated without a reference electrode, and were polarized at a constant anodic current density of 1.0 A cm^{-2}. BD-UNCD films deposited on both smooth and roughened Si, Ta, Nb, W, and Ti substrates were tested.

2.4 Electrochemical oxidation experiments

Reaction rates for TCE oxidation were measured under galvanostatic conditions in 50 mL of a 16-mM K_2SO_4 electrolyte at pH 8 after applied charges of 1, 50, and 100 A h cm^{-2}. The temperature was controlled at 22 °C using a circulating water bath. Currents and electrode potentials were controlled and monitored using a Gamry Series G 750 potentiostat/galvanostat. The BD-UNCD electrodes were mounted in the electrode holders described previously. A Princeton Applied Research (PAR) model 316 rotating disk electrode (RDE) assembly was used to rotate the electrodes at 3,000 rpm to eliminate mass transfer limitations on reaction rates. The counter electrode was a 12-cm long by 0.3-mm diameter Pt wire wrapped in a Nafion® membrane (Fuel Cell Scientific, Stoneham, MA) to isolate anodic and cathodic reactions. The reference electrode was a PAR Hg/Hg_2SO_4 electrode saturated with K_2SO_4. Potentials were reported versus the standard hydrogen electrode (SHE), after correction for solution resistance. To prevent the accumulation of adsorbed organic compounds on the electrode surface, the BD-UNCD electrode was preconditioned in the electrolyte solution at a current density of 20 mA cm^{-2} for 10 min before each experiment. Duplicate oxidation experiments were performed at a constant TCE concentration of 9.7 mM by purging the electrolyte solution with 50 mL min^{-1} of N_2 gas saturated with TCE at 22 °C. Constant aqueous TCE concentrations resulted from the high mixing rate provided by the RDE and the high purge rate of TCE into the solution so that the gas to liquid transfer rate of TCE ranged from 1.5 to 2 orders of magnitude greater than TCE oxidation rates. TCE oxidation

rates were calculated by the measurement of Cl^- accumulation in solution with time [12].

2.5 Electrochemical characterization methods

BD-UNCD films were characterized electrochemically using CV and EIS at 22 °C. CV and EIS experiments were conducted using the same experimental setup as described for the electrochemical oxidation experiments. CV experiments were conducted with a stationary electrode in a 1-M $NaClO_4$ background electrolyte in both the absence and presence of a 5-mM $Fe(CN)_6^{3-/4-}$ redox couple. The potential was swept at a scan rate of 100 mV s^{-1}. EIS experiments were conducted with the electrode rotating at 3,000 rpm in a 1-M $NaClO_4$ and 5-mM $Fe(CN)_6^{3-/4-}$ electrolyte composition. EIS measurements were made at the open circuit potential ($\sim$0.465 V/SHE) with an amplitude of $\pm$10 mV and over a frequency range of 0.1–3 $\times$ 10^5 Hz.

2.6 Analytical methods

Concentrations of Cl^- were determined by ion chromatography (Dionex ICS-3000). XPS measurements were performed at the University of Arizona Laboratory for Electron Spectroscopy and Surface Analysis. After the ageing tests, the electrodes were sent to Advanced Diamond Technologies to evaluate any surface morphology and surface chemistry changes using SEM and Raman spectroscopy.

3 Results and discussion

3.1 Electrode stability tests

Initial electrode stability tests were used to determine if delamination of the BD-UNCD films occurred after a 1.0 A h cm^{-2} applied charge. It was found that the surface roughness of the substrate was a key factor that determined the adhesion of the BD-UNCD film. A roughened substrate surface reduces the thermal stress within the BD-UNCD film and improves film adhesion to the substrate [13]. BD-UNCD films showed no visual signs of delamination on the roughed substrates except Ti. BD-UNCD films deposited on both rough and smooth Ti substrates rapidly delaminated and visible oxidation of the Ti substrate also occurred after 1 A h cm^{-2} applied charge. The poor adhesion of diamond to Ti has been documented in the literature [14–16]. Delamination of BD-UNCD films deposited on smooth Nb and W substrates also occurred, but films deposited on rough Nb and W substrates were stable. Further testing was conducted only on BD-UNCD films deposited on roughened Si, Ta, Nb, and W substrates.

3.2 Physical characterization

3.2.1 SEM measurements

SEM was used to characterize changes in the surface morphology and film thickness of the BD-UNCD film as a result of the charge applied to each electrode. Micrographs are shown for BD-UNCD/Si, BD-UNCD/Ta, and BD-UNCD/W (Fig. 1) and BD-UNCD/Nb (Fig. 2), which show SEM scans at two spots on each electrode. The "exposed" and "unexposed" areas, labeled in the figures, represent portions of the film that were either exposed or unexposed to the electrolyte solution during ageing experiments. Significant changes in the film morphology for the exposed area relative to the unexposed area were observed for BD-UNCD electrodes deposited on Si, Nb, and W substrates, whereas films deposited on Ta did not show a significant change.

The BD-UNCD/Si electrode after 100 A h cm^{-2} applied charge showed a textural change on the exposed area, which appears to be a result of electrochemical polishing (Fig. 1a). The exposed area shows less topographical variation than the unexposed area and also a needle-like crystal structure. Similar results have been obtained using BD-MCD film electrodes, where extensive polarization at 1.0 A cm^{-2} resulted in smoothing of the diamond surface [17]. Cross-sectional analysis of the BD-UNCD/Si electrode is provided in Fig. 3. It is clear from the results of SEM measurements taken across the entire diameter of the electrode that there was not any significant film deterioration (Fig. 3c). Therefore, the visual changes in the electrode surface depicted in Fig. 1a were only surficial and did not result in measureable film wear. The possible mechanism of electrochemical polishing of the BD-UNCD/Si electrode is discussed in Sect. 3.5.

The BD-UNCD/Nb electrode showed significant film delamination after 100 A h cm^{-2}. SEM micrographs shown in Fig. 2 highlight large areas where the BD-UNCD film is completely absent. These areas show an amorphous texture, which most likely is Nb_2O_5 oxide that was formed by electrochemical oxidation of the substrate.

The BD-UNCD/W electrode was only polarized to an applied charge of 50 A h cm^{-2}, because it was obvious by visual inspection that the BD-UNCD film was completely absent. SEM micrographs of this electrode at 50 A h cm^{-2} confirm this conclusion (Fig. 1c), showing that the BD-UNCD film is completely delaminated in the area that was exposed to solution.

3.2.2 Raman spectroscopy

Raman spectroscopy was used to characterize the bulk chemical composition of the BD-UNCD films as a function

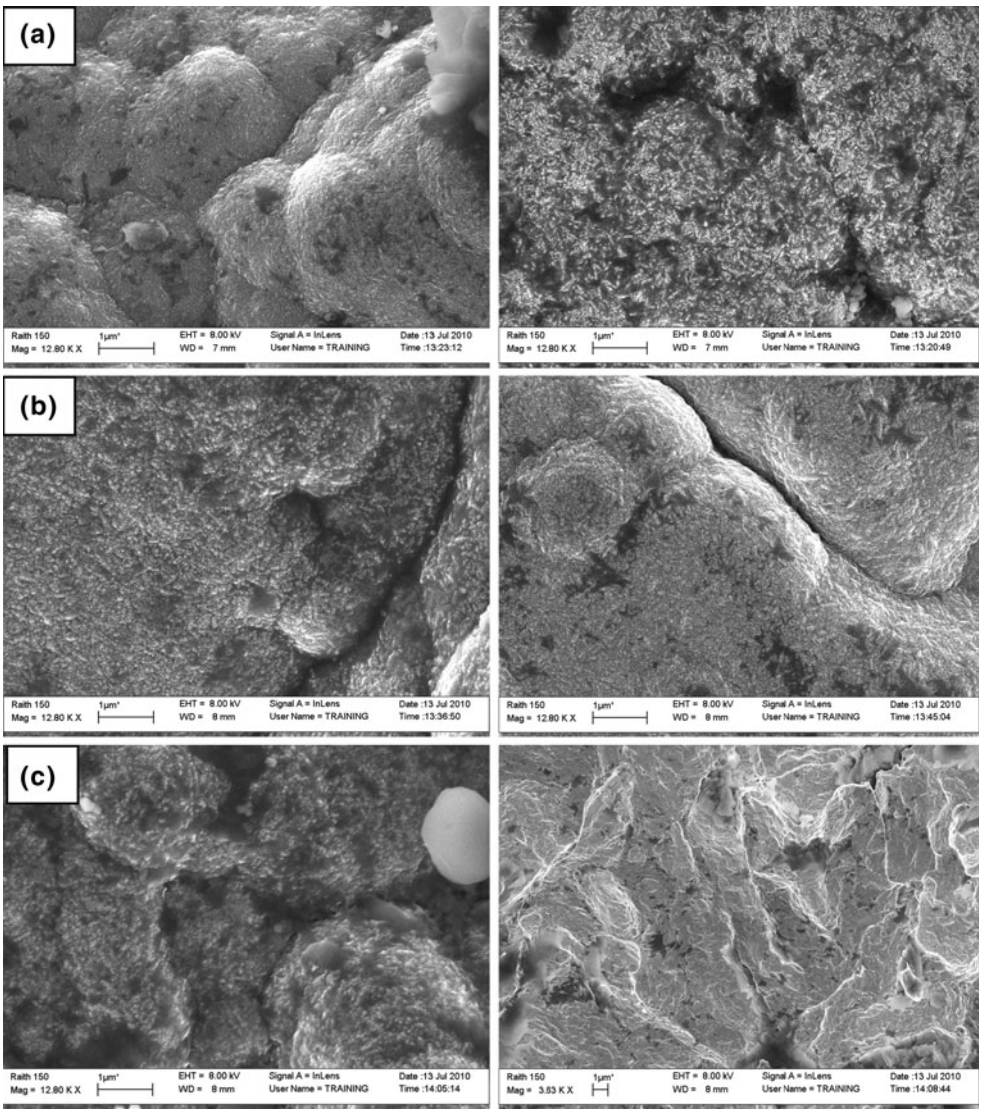

Fig. 1 SEM micrographs of BD-UNCD electrodes after an applied charge of 100 A h cm^{-2}. *Left image* is "unexposed" area and *right image* is "exposed" area to solution. **a** Si, **b** Ta, and **c** W

of the applied charge. In general, significant changes in the Raman spectra were only observed for the electrodes that delaminated (W and Nb). Both the BD-UNCD films deposited on Si and Ta show similar Raman spectrum between the exposed and unexposed areas of the film after an applied charge of 100 A h cm^{-2}. This result is consistent with the SEM observations and indicates that bulk changes to the BD-UNCD films did not occur as a result of anodic polarization.

3.2.3 XPS analysis

To characterize changes in the surface functional groups of the BD-UNCD film, XPS analysis was performed on both freshly prepared and aged electrodes. Peak assignments were chosen based on literature values [18], and a summary of XPS results is shown in Table 1. The as-deposited BD-UNCD films showed a high surface content of sp^3 C, ranging from 62.2 to 71.4% hydrogenated (C–H sp^3) and 14.2–27.5% non-hydrogenated (C sp^3) diamond. The as-deposited BD-UNCD films had a low surface content of graphitic sp^2 C (2.3–2.7%), and C–OH (5.5–9.1%) and C=O (2–4%) functional groups. These results are similar to measurements made on as-deposited BD-MCD films by other research groups [19–21].

High applied charges resulted in significant changes to the surface chemistry of all electrodes. For the BD-UNCD/Nb and BD-UNCD/W electrodes, the support was detected at molar ratios of 0.74 Nb:C and 3.51 W:C, respectively. These results support both SEM and Raman spectroscopy measurements discussed earlier, indicating BD-UNCD film delamination. The remaining C on Nb and W substrates consisted of reduced levels of sp^3 C and a higher content of oxygenated functional groups. As a result of anodic polarization, the overall O:C ratio increased from 0.08 and 0.06 to 1.10 and 1.00 for BD-UNCD/Nb and BD-UNCD/W

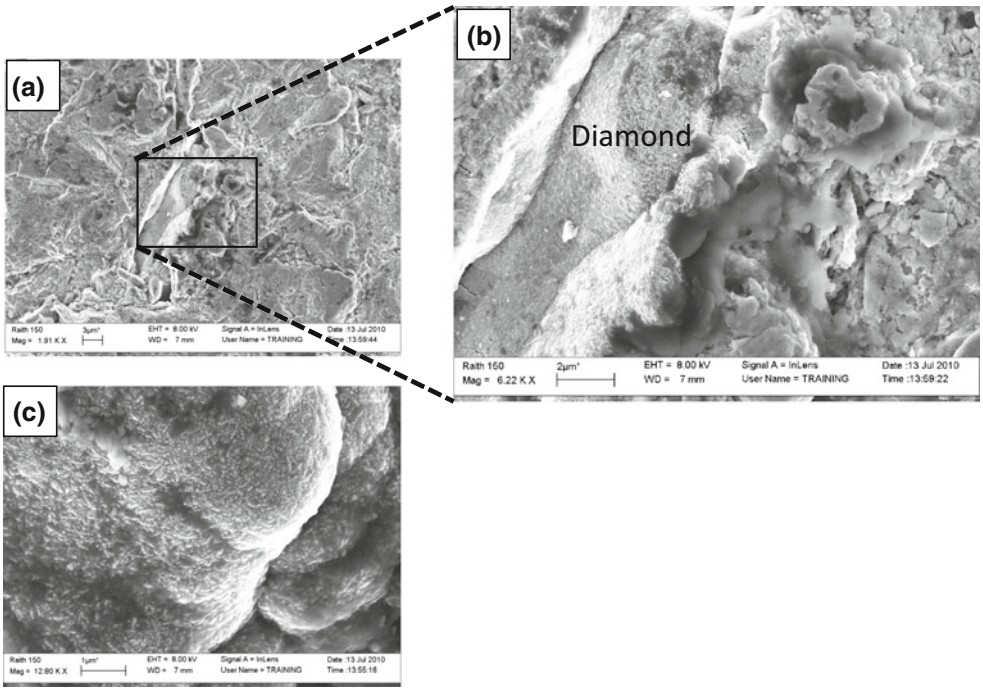

Fig. 2 SEM micrographs of BD-UNCD/Nb electrode after an applied charge of 100 A h cm^{-2} showing: **a** electrode area "exposed" to the solution, **b** blowup of (**a**) showing remaining diamond, and **c** electrode area "unexposed" to solution

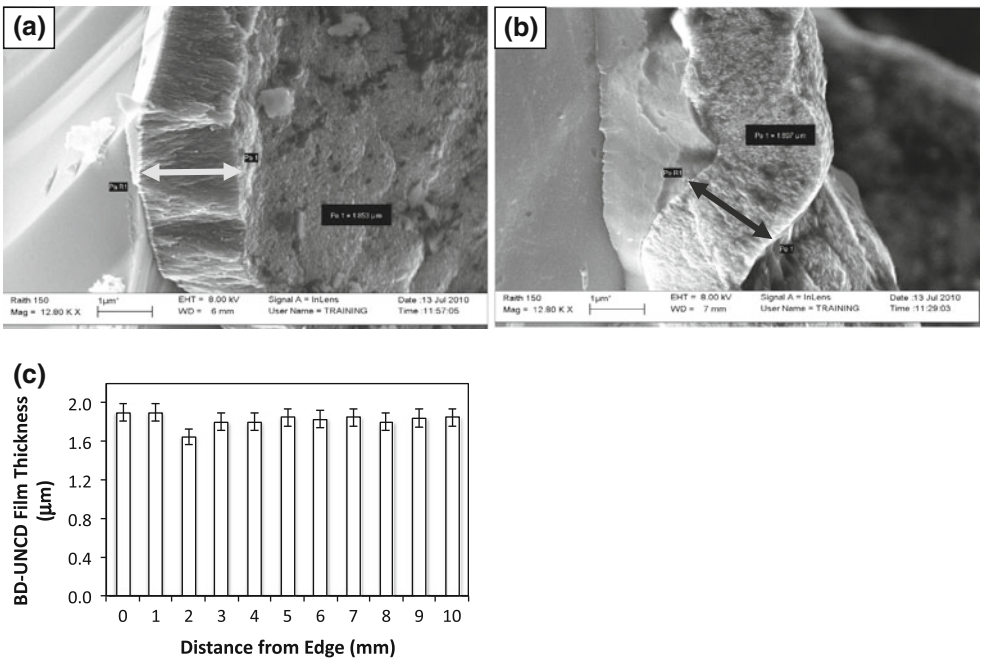

Fig. 3 SEM micrograph of cross-section of BD-UNCD/Si electrode after an applied charge of 100 A h cm^{-2} showing: **a** electrode area unexposed to the solution, and **b** electrode area exposed to solution. **c** Graph showing SEM cross-sectional BD-UNCD film thickness measurements at discrete points across the entire diameter of the electrode. Error bars represent 95% confidence intervals on measurements

electrodes, respectively. XPS measurements performed on BD-UNCD/Si and BD-UNCD/Ta electrodes did not detect the underlying substrate, but did show an increase in the overall oxygen content. The O:C ratio increased from 0.07 (BD-UNCD/Si) and 0.08 (BD-UNCD/Ta) for as-deposited electrodes to 0.27 (BD-UNCD/Si) and 0.24 (BD-UNCD/Ta) for electrodes after an applied charge of 100 A h cm^{-2}. The changes in the BD-UNCD films surficial chemical

Table 1 Summary of XPS data collected for BD-UNCD electrodes

Substrate	Applied charge (A h cm^{-2})	O:C ratio	Support:C ratio	Percent carbon					
				C sp^2	C–H (sp^3)	C–C (sp^3)	C–OH	C=O	Carboxyl or ester
Nb	0	0.08	0.00	2.3	71.4	14.2	9.1	2	–
Nb	100	1.10	0.74	–	11.8	32.3	24.3	19	12.6
W	0	0.06	0.00	2.7	69.4	22.2	5.7	–	–
W	50	1.00	3.51	–	–	46.5	35.6	17.8	–
Si	0	0.07	0.00	2.6	62.9	21.4	9	4	–
Si	100	0.27	0.00	2.6	34.7	33.9	16.1	8.9	3.8
Ta	0	0.08	0.00	2.3	62.2	27.5	5.5	2.4	–
Ta	100	0.24	0.00	2.7	36.2	30.3	15.9	9.5	5.5

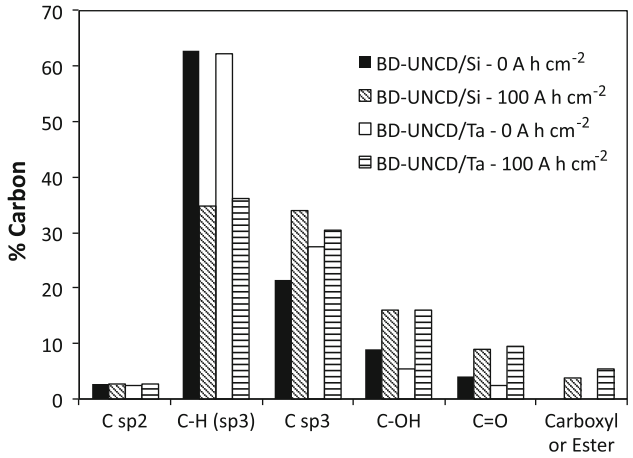

Fig. 4 Surface functional groups as determined by XPS spectra. Carbon percentages determined for BD-UNCD film electrodes deposited on Si and Ta substrates as a function of the applied charge

compositions as measured by XPS are illustrated in Fig. 4. A decrease in the C–H sp^3 content was associated with an increase in C–OH and C=O functional groups, and also the emergence of carboxyl or ester groups. These results are typical for electrochemically oxidized BD-MCD films that are subjected to low applied charges of $\leq$1 C cm^{-2} [19–22]. However, in our study, the BD-UNCD/Si and BD-UNCD/Ta electrodes were subjected to an applied charge of 360,000 C cm^{-2}, documenting that the surface chemistry of the films was similar to those reported in the literature subjected to much lower applied charges. Reports in the literature pertaining to XPS characterization of either BD-MCD or BD-UNCD electrodes after extreme anodic treatment could not be found.

Interestingly, an increase in the C sp^3 content was observed for the BD-UNCD/Si electrode after a 100 A h cm^{-2} applied charge. This result may be because of the electrochemical polishing that was observed by SEM for this electrode (Fig. 1a). The polishing of the electrode surface would reduce the surface roughness, which in turn would increase the fraction of high-coordinated sites (e.g., terraces) relative to low-coordinated sites (e.g., steps, kinks, and edges). Because XPS has a depth of penetration of a few atomic layers, such a change would result in a relative increase in the C sp^3 ratio.

3.3 Electrochemical characterization

3.3.1 CV measurements

To assess changes in the charge transfer occurring at the electrode surface, CV scans were performed on aged electrodes in a 1-M $NaClO_4$ electrolyte in the absence and presence of 5-mM concentrations of the $Fe(CN)_6^{3-/4-}$ redox couple. Scans in 1-M $NaClO_4$ are shown in Fig. 5. An oxidation peak (O-1) at 2.4–2.5 V/SHE and reduction peak (R-1) at −0.9 to −1.4 V/SHE are present for all four electrodes at an applied charge of 1.0 A h cm^{-2}. Peaks are attributed to graphitic micro-domains of sp^2 carbon that are likely deposited at the diamond grain boundaries. The high faradic current response associated with these peaks are attributed to the very small grain size of the BD-UNCD films ($\sim$1 to 3 nm), thus creating additional sites for sp^2 carbon deposition relative to BD-MCD. Previous study involving grafting of highly ordered pyrolytic graphite (HOPG) to BD-MCD electrodes produced an oxidation peak at about 1.9–2.0 V/SHE and a reduction peak that occurred anywhere from 1.3 to 0.1 V/SHE [23]. The shifting of the reduction peak was attributed to lattice distortion of the HOPG [23]. The position of the reduction peak R-1 (shown in Fig. 5) occurs at a much more negative potential than previously reported, which is likely because of the presence of highly distorted graphitic micro-domains on the BD-UNCD surface relative to the HOPG used by Mahe et al. [23]. An additional oxidation peak (O-2) observed on BD-UNCD films deposited on Nb and W substrates at an applied charge of 1.0 A h cm^{-2} was observed at $\sim$1.3 V/SHE (Fig. 5c, d), which is also attributed to graphitic carbon in a different bonding environment.

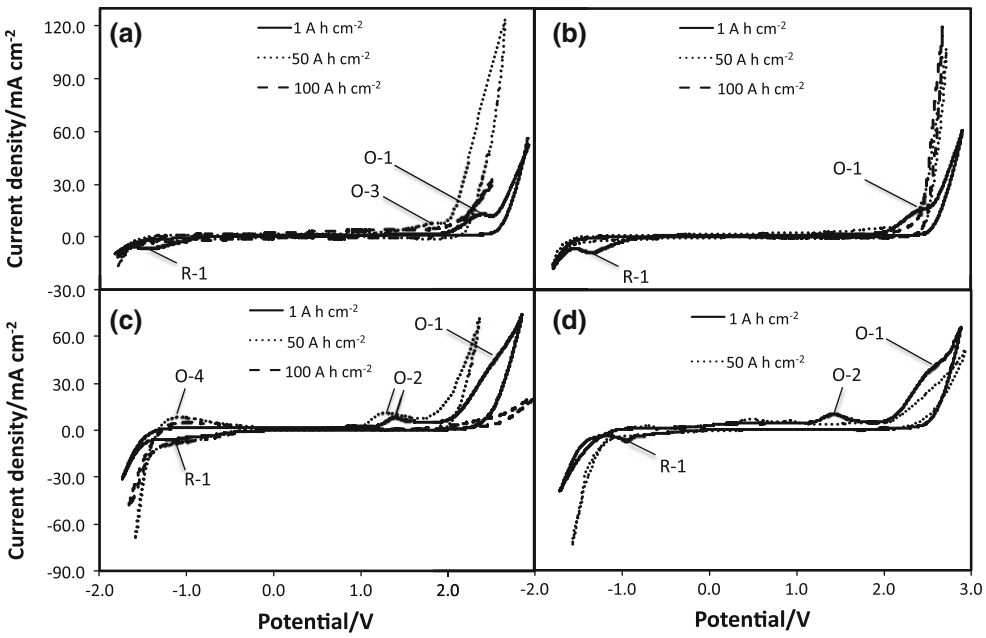

Fig. 5 CV scans of electrodes in 1-M $NaClO_4$ at different applied charges: **a** Si, **b** Ta, **c** Nb, and **d** W

On ageing the electrodes to an applied charge of 50 A h cm^{-2}, peaks O-1 and R-1 are no longer present on CV scans for any of the electrodes (Fig. 5), indicating that they were oxidized from the surface. However, additional oxidation peaks were detected on the BD-UNCD/Si (O-3) and BD-UNCD/Nb (O-4) electrodes at approximately 1.8 and −1.0 V/SHE, respectively (Fig. 5a, c). Peak O-3 was once again attributed to graphitic carbon, and O-4 is thought to be because of the response of the Nb support, which was detected by both SEM and XPS measurements. Two additional oxidation peaks and a reduction peak were also observed on the BD-UNCD/W electrode at an applied charge of 50 A h cm^{-2}, as shown in Fig. 6. These peaks are attributed to the electrochemical response of the W support, which was detected by SEM and XPS measurements.

On further ageing of the Si, Ta, and Nb electrodes to 100 A h cm^{-2}, the potential for oxygen evolution of the BD-UNCD/Si and BD-UNCD/Nb electrodes increased and peaks O-3 and O-2 were eliminated, respectively. The increased potential for oxygen evolution is clearly a result of BD-UNCD delamination from the Nb support, and may be attributed to the morphology changes that were observed by SEM (Fig. 1a) for the BD-UNCD/Si electrode. The BD-UNCD/Ta electrode showed an identical response at both 50 and 100 A h cm^{-2} (Fig. 5b).

Results from CV scans performed in 1-M $NaClO_4$ solutions containing 5-mM $Fe(CN)_6^{3-/4-}$ are shown in Fig. 7. The BD-UNCD/Si electrode showed a significant increase in peak separation for the $Fe(CN)_6^{3-/4-}$ redox couple after the passage of 100 A h cm^{-2}, whereas the BD-UNCD/Ta electrode did not show a change. The surface chemistry of both electrodes

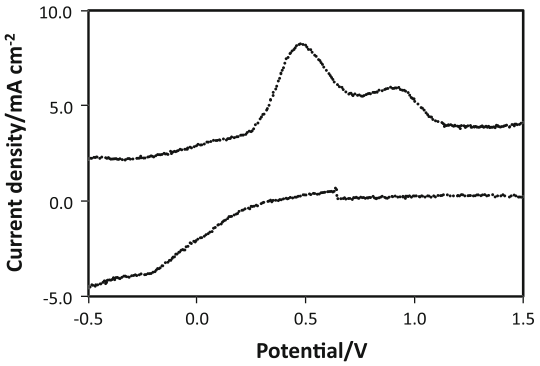

Fig. 6 CV scans of BD-UNCD/W electrode in 1-M $NaClO_4$ at an applied charge of 50 A h cm^{-2}

determined by XPS measurements was virtually identical at 100 A h cm^{-2} (see Table 1; Fig. 4). Therefore, the changes in the CV scans on ageing are thought to be a result of the morphology changes that were observed by SEM (see Fig. 1a). The BD-UNCD/Nb electrode showed a decrease in the response of the $Fe(CN)_6^{3-/4-}$ redox couple with ageing. There was not any measurable response at 100 A h cm^{-2} because of BD-UNCD delamination. Surprisingly, the response of the BD-UNCD/W electrode was nearly identical at 1 and 50 A h cm^{-2} despite complete delamination of the BD-UNCD film. This result is an indication that the oxidized W is still electro-active, and that both the BD-UNCD film and the oxidized W show reversible metallic behavior for the $Fe(CN)_6^{3-/4-}$ redox couple. Reports in the literature indicate that WO_3-based electrodes are active for organic compound oxidation [24].

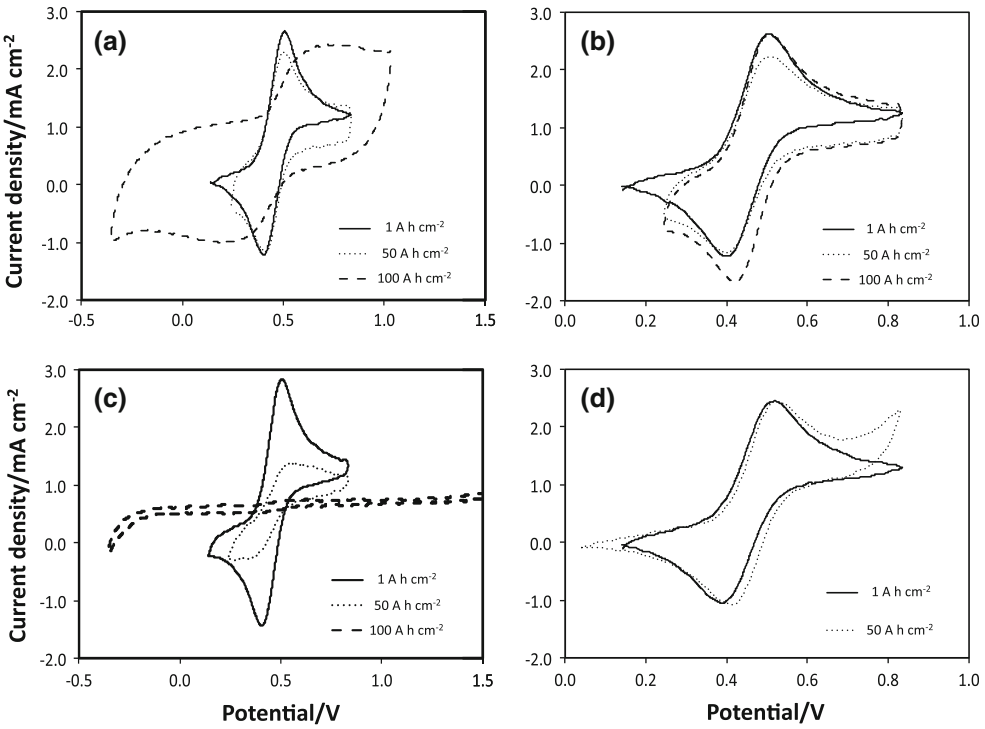

Fig. 7 CV scans of BD-UNCD film electrodes at different applied charges in a 1-M $NaClO_4$/5-mM $K_3[FeCN_6]$/ 5-mM $K_4[FeCN_6]$ electrolyte. BD-UNCD films were deposited on roughened **a** Si, **b** Ta, **c** Nb, and **d** W

3.3.2 EIS measurements

EIS scans were performed on as-deposited electrodes and after an applied charge of 100 A h cm^{-2} to characterize electron transfer at the BD-UNCD surface. Experiments were performed in a 1-M $NaClO_4$ background electrolyte containing 5 mM of the $Fe(CN)_6^{3-/4-}$ redox couple. The $Fe(CN)_6^{3-/4-}$ redox couple was chosen because it has been shown to be sensitive to chemical changes at the electrode surface [23]. EIS scans shown in Fig. 8 were fit using the two equivalent circuit models shown in Fig. 9. The first model shown in Fig. 9a contains the following elements: solution resistance (R_s), charge transfer resistance (R_{ct}), and the double layer capacitance (C_{dl}) was replaced with a constant phase element (CPE_{dl}) to account for surface roughness and reactive site heterogeneity [25]. The equivalent circuit shown in Fig. 9b also includes an additional resistance element that corresponds to a non-conductive passive layer (R_p) along with an additional CPE (CPE_p). Similar equivalent circuit models have been used to model EIS data for BD-MCD [26] and UNCD electrodes [27]. The summary of values for model parameters is shown in Table 2. The EIS spectrum for the as-deposited electrodes and the BD-UNCD/Ta electrode after a 100 A h cm^{-2} applied charge was fit using the equivalent circuit shown in Fig. 9a. The similarity in values shown in Table 2 for the as-deposited and the aged BD-UNCD/Ta electrodes indicates that the film was not compromised during anodic polarization. It should be noted that the CPE_{dl} values found for the as-deposited and aged BD-UNCD/Ta electrodes were approximately three orders of magnitude higher than those reported for BD-MCD electrodes [26]. This very high capacitance is likely related to the enhanced surface area, relative to MCD, present at the numerous UNCD grain boundaries. However, the EIS spectrum for the aged BD-UNCD/Si and BDD-UNCD/Nb electrodes was fit with the model shown in Fig. 9b, with values of 68.2 ± 1.4 and 1,421 ± 3 Ω cm^2 for R_p, respectively. The relatively low R_p value for the BD-UNCD/Si electrode is a result of physical and chemical changes to the BD-UNCD film surface that were observed by SEM and CV measurements. The large value obtained for R_p for the BD-UNCD/Nb electrode was a result of the delamination of large portions of the BD-UNCD film that were evidenced by SEM. The corresponding passive layer corresponds to the formation of Nb_2O_5 oxide on the exposed support. For all fits, the values for n_{dl} and n_p were between 0.74 and 0.89, which are in the range typical for rough electrodes with a fractal dimension of 2.35 and 2.12, respectively [28], which is indicative of the electrodes used in this study. The EIS data for the BD-UNCD/W electrode (Fig. 8d) did not fit the models shown in Fig. 9, because of the complete delamination of the BD-UNCD film and the unique electrochemical properties of the WO_3 substrate that formed.

3.4 TCE oxidation

Electrochemical oxidation of TCE was performed using all four electrodes as a function of the applied charge. Results

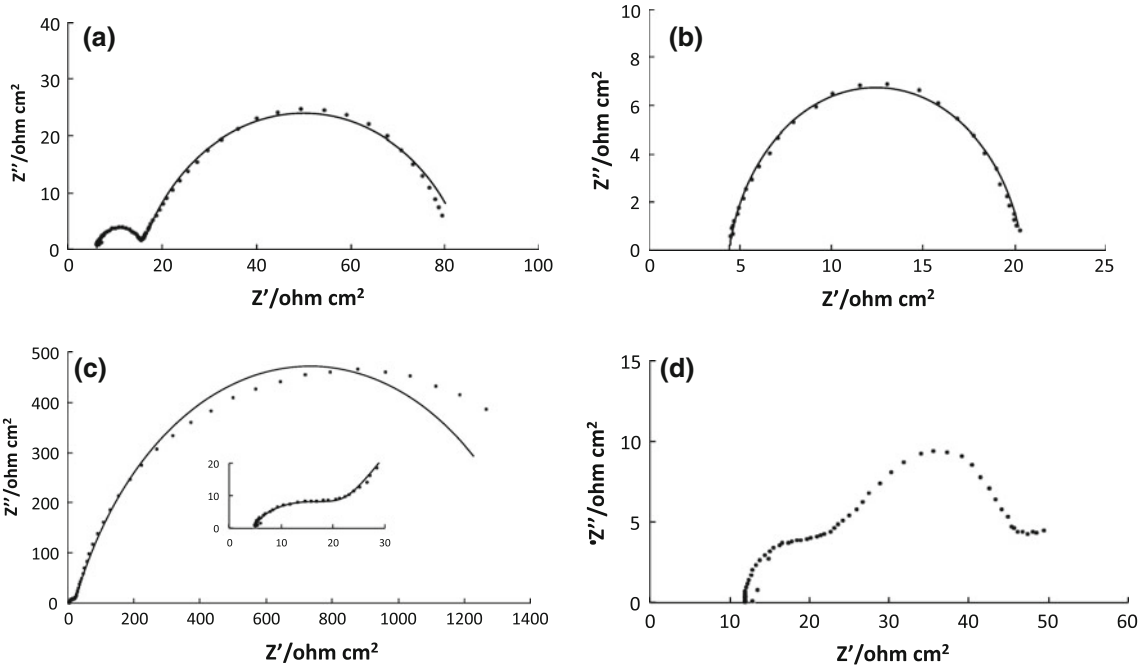

Fig. 8 EIS scans of electrodes in a 1-M $NaClO_4$/5-mM $K_3[FeCN_6]$/5-mM $K_4[FeCN_6]$ electrolyte after an applied charge of 100 A h cm^{-2}: **a** Si, **b** Ta, **c** Nb, and **d** W. *Symbols* represent measured data and *solid lines* represent model fit of equivalent circuit model shown in Fig. 9

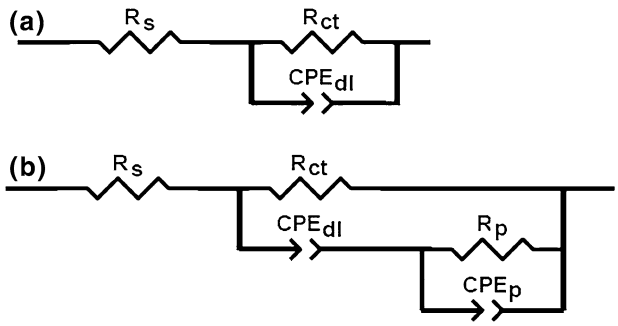

Fig. 9 Equivalent circuit models used to fit the data shown in Fig. 8

from these experiments are shown in Fig. 10. TCE oxidation with electrodes having applied charges of 1 and 50 A h cm^{-2} showed approximately a linear increase in the TCE oxidation rate with increasing potential. The notable exception to this observation is the BD-UNCD/W electrode that changed from a linear increase in TCE oxidation rate at a 1.0 A h cm^{-2} applied charge to an exponential increase in the TCE oxidation rate at a 50 A h cm^{-2} applied charge. This change is indicative of a switch in the mechanism of TCE oxidation from a hydroxyl radical–mediated oxidation (1.0 A h cm^{-2}) for BD-UNCD to a direct electron transfer oxidation (50 A h cm^{-2}) for WO_3 [29]. As noted previously, reports in the literature indicate that WO_3-based electrodes are active for organic compound oxidation [24].

At a 100 A h cm^{-2} applied charge, the TCE oxidation rates for the BD-UNCD/Si, BD-UNCD/Ta, and BD-UNCD/Nb electrodes were only weakly correlated to the electrode potential. For the BD-UNCD/Nb electrode, this result was attributed to delamination of large portions of the BD-UNCD film. However, for the BD-UNCD/Si and BD-UNCD/Ta electrodes, the BD-UNCD film was intact. For the BD-UNCD/Si electrode, the slow TCE oxidation rates may be a result of the morphology changes indicated by SEM. However, it seems more likely that the electronic properties of the BD-UNCD film changed because of the applied polarization. The characterization of BD-MCD films using conductive probe-atomic force microscopy (CP-AFM) and scanning electrochemical microscopy (SECM) allowed conductivity mapping of the electrode surface [30]. Results from their study indicate that the films consist primarily of insulating diamond containing isolated conductive sites (~10 to 60% of geometric surface area) [30]. Evidence suggests that these conductive sites were concentrated at grain boundaries [30], which confirmed previous work that boron concentrates at grain boundaries [31]. Reports in the literature suggest that anodic polarization can lead to a depletion of H in the surficial diamond film, which initially leads to electrode passivation because of the migration of H into the bulk film and the depletion of boron acceptors by formation of B–H pairs [32, 33]. However, extended polarization has been proposed to cause dissociation of B–H pairs and thus an increase in the boron acceptors and subsequent increase in conductivity [34]. These processes, accompanied by the formation of various oxygenated functional groups on the electrode

Table 2 Summary of fitted values used to fit the equivalent circuit model shown in Fig. 8 for EIS data shown in Fig. 7

Electrode	R_s (Ω cm^2)	R_{ct} (Ω cm^2)	CPE_{dl} (μF cm^{-2} s^{n-1})	n_{dl}	R_p (Ω cm^2)	CPE_p (mF cm^{-2} s^{n-1})	n_p
BD-UNCD[a]	8.66 ± 0.30	11.09 ± 0.47	(5.43 ± 0.08) × 10^3	0.77 ± 0.04	–	–	–
BD-UNCD/Si	6.03 ± 0.09	9.98 ± 0.24	21.9 ± 4.94	0.80 ± 0.02	68.2 ± 1.4	3.09 ± 0.11	0.77 ± 0.01
BD-UNCD/Nb	4.89 ± 0.08	18.33 ± 0.56	8.40 ± 1.43	0.87 ± 0.10	1,421 ± 3	0.297 ± 0.006	0.74 ± 0.05
BD-UNCD/Ta	4.41 ± 2.00	15.99 ± 0.18	(6.17 ± 0.20) × 10^3	0.89 ± 0.08	–	–	–

Errors represent 95% confidence interval on fitted values

[a] Represents the average values found for the equivalent circuit fits of as-deposited BD-UNCD films on Si, Nb, and Ta prior to anodic polarization

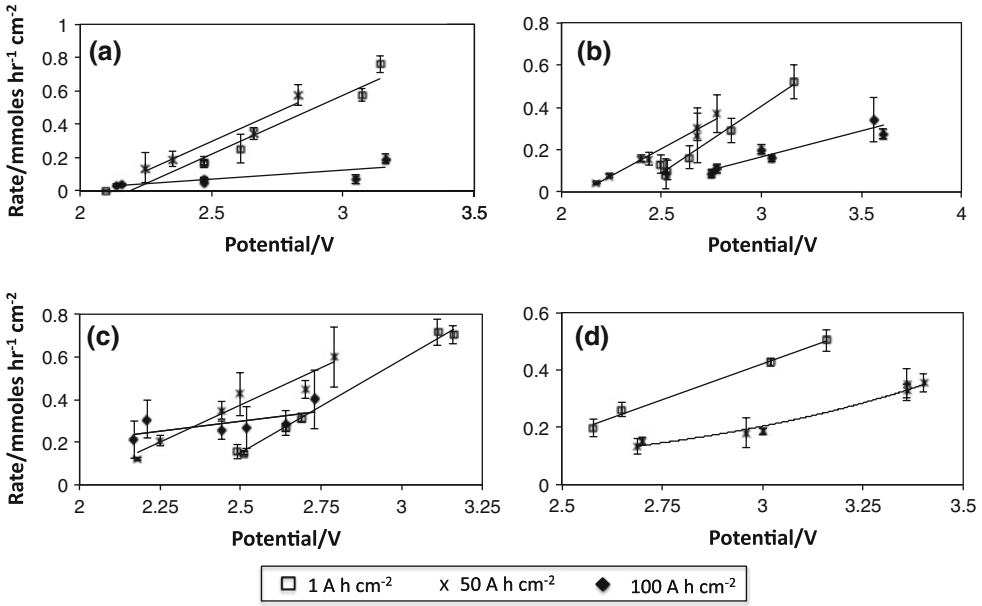

Fig. 10 Rates of TCE oxidation as a function of potential and electrode ageing. **a** BD-UNCD/Si: Regression—1 A h cm^{-2}: $y = 0.71x - 1.55$, $R^2 = 0.94$; 50 A h cm^{-2}: $y = 0.71x - 1.47$, $R^2 = 0.96$; 100 A h cm^{-2}: $y = 0.11x - 0.20$, $R^2 = 0.63$; **b** BD-UNCD/Ta: Regression—1 A h cm^{-2}: $y = 0.63x - 1.49$, $R^2 = 0.98$; 50 A h cm^{-2}: $y = 0.51x - 1.08$, $R^2 = 0.98$; 100 A h cm^{-2}: $y = 0.25x - 0.57$, $R^2 = 0.90$; **c** BD-UNCD/Nb: Regression—1 A h cm^{-2}: $y = 0.88x - 2.04$, $R^2 = 0.99$; 50 A h cm^{-2}: $y = 0.70x - 1.37$, $R^2 = 0.94$; 100 A h cm^{-2}: $y = 0.19x - 0.17$, $R^2 = 0.44$; **d** BD-UNCD/W: Regression—1 A h cm^{-2}: $y = 0.50x - 1.08$, $R^2 = 0.99$; 50 A h cm^{-2}: $y = 0.004e^{(1.34x)}$, $R^2 = 0.97$. Best fit lines represent linear or exponential regression

surface, can result in altering electrochemically active sites, which alters electron transfer for different adsorbed compounds (e.g., water, TCE). The relationship is complex and more research is needed to fully understand the mechanisms that control electron transfer at the BDD surface.

3.5 Proposed mechanisms of electrode wear

Results indicate that the main mode of electrode wear was associated with electrochemical corrosion of the support, and not oxidation of the BD-UNCD film. Table 3 provides a summary of the standard electrode potential (E^o) and the coefficient of thermal expansion (CTE) for the oxidation of the metal substrates used in this study (i.e., Si, Ta, Nb, W, and Ti). High values for electrode potential indicate that the substrate will be rapidly oxidized when polarized to an anodic potential. However, the key factor that determines the BD-UNCD film adhesion to the substrate is related to the CTE value. The most important factor is matching the CTE value for diamond (CTE = 1.18 × 10^{-6} C^{-1} [35]) and the substrate, which is essential to maintain film adhesion as the electrode cools to room temperature after film deposition. A large difference between the CTE value of diamond and the substrate can cause defects in the film that allow electrolyte permeation through the diamond film and lead to corrosion of the substrate. If the CTE value decreases from the metal substrate to its corresponding oxide, then the oxide is more compact and will not result in delamination of the BD-UNCD film. This scenario is the case for Si and Ta, which correlated to the most stable electrodes tested. A CTE increase from the metal to the oxide results in a physical expansion of the oxide that promotes BD-UNCD delamination. This scenario was the case for Nb, W, and Ti, which resulted in BD-UNCD film

Table 3 Summary of electrode potential and coefficient of thermal expansion (CTE) for metal substrates used for the deposition of BD-UNCD films

Reaction	E^o (V)	CTE ($\times 10^6$ C^{-1}) (metal [35]/oxide)
Si/SiO_2	−0.86	2.5/0.5 [38]
Ta/Ta_2O_5	0.75	6.4/3.6 [39]
Nb/Nb_2O_5	0.73	7.3/7.7 [39]
W/WO_3	0.09	4.5/5.7 [40]
Ti/TiO_2	2.13	8.6/9.9 [41]

delamination. Additionally, roughening the substrate by a bead blast method can result in greater adhesion, because of increasing the density of nucleation sites for the BD-UNCD film and reducing the overall film stress [13].

Although film delamination did not occur for the BD-UNCD/Si electrode, both the physical and electrochemical characteristics changed as a function of anodic oxidation. SEM images taken after the passage of 100 A h cm^{-2} clearly showed electrochemical polishing occurred on the surface of the BD-UNCD film (Fig. 1a). After passing 100 A h cm^{-2} charge, this electrode also showed an increased potential for water oxidation (Fig. 5a) and an increased peak separation of the $Fe(CN)_6^{3-/4-}$ redox couple (Fig. 7a), relative to measurements performed after passage of 50 A h cm^{-2}. Changes in the electrochemical response of the BD-UNCD/Si electrode are likely correlated with electrochemical polishing. As discussed in Sect. 3.2.2, changes to the surface roughness can alter the coordination number of active sites and thus their electrochemical response. Reports in the literature indicate that surface roughness has a substantial effect on oxidation reactions [36]. However, it remains unclear whether the Si substrate influences electrochemical polishing of the BD-UNCD surface. XPS measurements have detected low levels of Si ($\sim$0.5 atomic % as Si–C and C–Si–O species) on the surface of BD-MCD/Si electrodes, and it was suggested that Si diffused from the substrate along diamond grain boundaries to the BD-MCD surface, as a result of the high temperature CVD process [18]. Although research has not been conducted regarding the role of Si–C species on BDD electrode wear, reports in the literature indicate that oxidation of Si–C can occur under similar voltages and temperatures used in our study, according to the following reaction [37]:

$$SiC + 4H_2O \rightarrow SiO_2 + CO_2 + 8H^+ + 8e^- \quad (1)$$

This process could explain the electrochemical polishing observed in our study, but more research is warranted, as a detailed XPS scan on the Si 2p region was not performed.

4 Conclusions

The performance and stability of BD-UNCD film electrodes on a variety of substrates (Si, Ta, Nb, W, and Ti) was investigated as a function of the applied anodic charge. A high current density of 1 A cm^{-2} was used to test the anodic stability of the BD-UNCD films, up to applied charges of 100 A h cm^{-2}. Anodic treatment of the electrodes resulted in oxidation of the BD-UNCD film surface, as determined by XPS measurements. Cross-sectional SEM measurements did not show any signs of film wear. However, it was found that substrate roughness, substrate electroactivity, and compactness of the corresponding substrate oxide were key parameters that affected film adhesion to the substrate. The primary mechanism of electrode failure was associated with delamination of the BD-UNCD film caused by oxidation of the substrate. Substrate materials whose oxides had a larger CTE relative to the reduced metal resulted in film delamination. The approximate substrate stability followed the order of: Ta > Si > Nb > W $\gg$ Ti.

Surficial changes as well as film delamination resulted in substantial changes in the electrochemical properties of the various electrodes as determined by CV, EIS, and TCE oxidation experiments. Interestingly, it was observed that WO_3 was active for the electrochemical oxidation of TCE after delamination of the BD-UNCD film from the W substrate. Results indicate that the mechanism of TCE oxidation shifted from a hydroxyl radical–mediated pathway for the BD-UNCD/W electrode to a direct electron transfer pathway for the WO_3 material, indicating future exploration of WO_3 electrodes is warranted for water treatment applications.

Acknowledgments We thank the National Science Foundation Small Business for Innovative Research program (NSF-IIP-0945935) for the financial support of this work. We also thank Craig Duncan and Laura-Ann Chin for conducting TCE oxidation experiments and Dr. Orchideh Azizi for performing EIS fits.

References

1. Kraft A (2007) Int J Electrochem Sci 2:355
2. Xu JS, Granger MC, Chen QY et al (1997) Anal Chem 69:A591
3. Bennett JA, Wang JA, Show Y et al (2004) J Electrochem Soc 151:E306
4. Jiao S, Sumant A, Kirk MA et al (2001) J Appl Phys 90:118
5. Krauss AR, Auciello O, Gruen DM et al (2001) Diam Relat Mater 10:1952
6. Naguib NN, Elam JW, Birrell J et al (2006) Chem Phys Lett 430:345
7. Auciello O, Pacheco S, Sumant AV et al (2007) IEEE Microw Mag 8:61
8. Ramanathan M, Darling SB, Sumant AV et al (2010) J Vac Sci Technol A 28:979

9. Sumant AV, Auciello O, Carpick RW et al (2010) MRS Bull 35:281
10. Iniesta J, Michaud PA, Panizza M et al (2001) Electrochim Acta 46:3573
11. Mishra D, Liao ZH, Farrell J (2008) Environ Sci Technol 42:9344
12. Carter KE, Farrell J (2009) Environ Sci Technol 43:8350
13. Lim PY, Lin FY, Shih HC et al (2008) Thin Solid Films 516:6125
14. Chen XM, Chen GH, Gao FR et al (2003) Environ Sci Technol 37:5021
15. Lowe MA, Fischer AE, Swain GM (2006) J Electrochem Soc 153:B506
16. Tian Y, Chen XM, Shang C et al (2006) J Electrochem Soc 153:J80
17. Duo I, Levy-Clement C, Fujishima A et al (2004) J Appl Electrochem 34:935
18. Ferro S, Dal Colle M, De Battisti A (2005) Carbon 43:1191
19. Simon N, Girard H, Ballutaud D et al (2005) Diam Relat Mater 14:1179
20. Wang M, Simon N, Decorse-Pascanut C et al (2009) Electrochim Acta 54:5818
21. Wang M, Simon N, Charrier G et al (2010) Electrochem Commun 12:351
22. Goeting CH, Marken F, Gutierrez-Sosa A et al (2000) Diam Relat Mater 9:390
23. Mahe E, Devilliers D, Comninellis C (2005) Electrochim Acta 50:2263
24. Bock C, MacDougall B (2002) Electrochim Acta 47:3361
25. Macdonald JR (1987) Impedance spectroscopy. Wiley, New York
26. Salazar-Banda GR, de Carvalho AE, Andrade LS et al (2010) J Appl Electrochem 40:1817
27. Hernando J, Lud SQ, Bruno P et al (2009) Electrochim Acta 54:1909
28. Mulder WH, Sluyters JH, Pajkossy T et al (1990) J Electroanal Chem 285:103
29. Bockris JOM, Reddy AK, Gambra-Aldeco M (2000) Modern electrochemistry, 2nd edn. Plenum Press, New York
30. Holt KB, Bard AJ, Show Y et al (2004) J Phys Chem B 39:15117
31. Kolber T, Piplits K, Haubner R et al (1999) Fresenius J Anal Chem 365:636
32. Tryk DA, Tsunozaki K, Rao TN et al (2001) Diam Relat Mater 10:1804
33. Kondo T, Honda K, Tryk DA et al (2005) J Electrochem Soc 152:E18
34. Ricci PC, Anedda A, Carbonaro CM et al (2005) Thin Solid Films 482:311
35. Haynes WM (2010) CRC handbook of chemistry and physics, 91st edn. CRC Press, New York
36. Canizares P, Saez C, Martinez F et al (2008) Electrochem Solid State 11:E15
37. Rysy S, Sadowski H, Helbig R (1999) J Solid State Electron 3:437
38. Scholze H (1990) Glass: nature, structure and properties. Springer, New York
39. Touloukian YS, Kirby RK, Taylor RE et al (1977) Thermal expansion, nonmetallic solids. Plenum, New York
40. Rosen C, Banks E, Post B (1956) Acta Crystallogr 9:475
41. Straumanis ME, Ejima T, James WJ (1960) Acta Crystallogr 13:1022